

In vivo magnetic resonance imaging of acute brain inflammation using microparticles of iron oxide

Martina A McAteer^{1,4}, Nicola R Sibson^{2,4}, Constantin von zur Muhlen¹, Jurgen E Schneider¹, Andrew S Lowe², Nicholas Warrick¹, Keith M Channon¹, Daniel C Anthony³ & Robin P Choudhury¹

Multiple sclerosis is a disease of the central nervous system that is associated with leukocyte recruitment and subsequent inflammation, demyelination and axonal loss. Endothelial vascular cell adhesion molecule-1 (VCAM-1) and its ligand, $\alpha_4\beta_1$ integrin, are key mediators of leukocyte recruitment, and selective inhibitors that bind to the α_4 subunit of $\alpha_4\beta_1$ substantially reduce clinical relapse in multiple sclerosis. Urgently needed is a molecular imaging technique to accelerate diagnosis, to quantify disease activity and to guide specific therapy. Here we report *in vivo* detection of VCAM-1 in acute brain inflammation, by magnetic resonance imaging in a mouse model, at a time when pathology is otherwise undetectable. Antibody-conjugated microparticles carrying a large amount of iron oxide provide potent, quantifiable contrast effects that delineate the architecture of activated cerebral blood vessels. Their rapid clearance from blood results in minimal background contrast. This technology is adaptable to monitor the expression of endothelial molecules *in vivo* in various pathologies.

Multiple sclerosis is a disease of the central nervous system characterized by multifocal white matter lesions¹. At present, the diagnostic criteria for multiple sclerosis, which incorporate both clinical and magnetic resonance imaging (MRI) characteristics, require the demonstration of lesion dissemination in both time and space^{2,3}. Transverse relaxation time (T_2)-weighted and gadolinium-enhanced longitudinal relaxation time (T_1)-weighted MRI detects some but not all lesions, whereas advanced MRI techniques such as diffusion imaging⁴, magnetization transfer⁵ and magnetic resonance spectroscopy⁶ may provide additional insights. These approaches are, however, limited in two key respects: first, they image downstream injury, reflecting relatively advanced pathology; and second, although they provide an indication of severity, they cannot accurately assess disease activity⁷. There is a pressing need for molecular imaging techniques that can identify early pathogenesis to accelerate accurate diagnosis and to guide specific therapy.

VCAM-1 and its ligand, $\alpha_4\beta_1$ integrin (also called very late antigen-4, VLA-4), are important mediators of mononuclear leukocyte recruitment and lesion initiation⁸. VCAM-1 is not constitutively expressed

on cerebral vascular endothelium, but is upregulated with endothelial activation⁹. Selective blockade of this interaction in experimental autoimmune encephalitis, the rodent analog of multiple sclerosis, results in abolition of both lymphocyte recruitment and the paralysis that usually follows¹⁰. Similarly, selective adhesion molecule inhibitors that bind to $\alpha_4\beta_1$ block its association with VCAM-1, resulting in a substantial reduction in both new or enlarging lesions on MRI and clinical relapse in multiple sclerosis¹¹. We reasoned that the sensitivity of MRI for detecting early inflammation might be enhanced by using a molecular contrast agent targeted to VCAM-1. Such an approach might potentially provide a more precise and earlier diagnosis, and insights into disease activity, prognosis and response to specific therapy.

Microparticles of iron oxide (MPIO, size range 0.76–1.63 μm) have been used for cellular imaging and tracking¹². For some molecular imaging applications, the size of these particles would preclude delivery to the target site. For imaging endovascular structures, however, MPIO possess several positive attributes. First, MPIO convey an amount of iron that is orders of magnitude greater than that conveyed by the ultrasmall particles of iron oxide (USPIO) that have been used previously for MRI contrast. Second, the effects of MPIO on local magnetic field homogeneity, and therefore on detectable contrast, extend for a distance roughly 50 times the physical diameter of the microparticle¹². Third, the size of MPIO means that these particles are less susceptible than USPIO to extravasation or non-specific uptake by endothelial cells and therefore they retain specificity for molecular targets¹³.

Accordingly, we have developed a VCAM-1 antibody-conjugated 1- μm MPIO that shows specific and quantitative binding to activated endothelial cells in culture. We report that, when coupled with MRI, this targeted MPIO contrast agent detects VCAM-1 expression *in vivo* in mouse brain inflammation with high specificity and exceptional conspicuity.

RESULTS

VCAM-MPIO bind to TNF- α stimulated sEND-1 cells *in vitro*

Monoclonal antibodies to VCAM-1 were conjugated to 1- μm diameter MPIO (hereafter called VCAM-MPIO). We tested the capacity of this construct for specific and quantitative binding *in vitro* on cells

¹Department of Cardiovascular Medicine, John Radcliffe Hospital, University of Oxford, Oxford OX3 9DU, UK. ²Experimental Neuroimaging Group, Department of Physiology, Anatomy and Genetics, Sherrington Building, Parks Road, Oxford OX1 3PT, UK. ³Department of Pharmacology, Mansfield Road, Oxford OX1 3QX, UK. ⁴These authors contributed equally to this work. Correspondence should be addressed to R.P.C. (robin.choudhury@cardiov.ox.ac.uk).

Received 24 May; accepted 13 July; published online 23 September 2007; doi:10.1038/nm1631

of a mouse endothelial line (sEND-1) that were exposed to graded doses of tumor-necrosis factor- α (TNF- α), an inflammatory stimulus used to provoke surface expression of VCAM-1. After extensive washing, antibody binding to MPIO was quantified under differential interference contrast microscopy. VCAM-MPIO was retained sparsely by unstimulated sEND-1 cells, reflecting low basal expression of VCAM-1. The number of VCAM-MPIO bound to sEND-1 cells increased in response to increasing doses of TNF- α (Fig. 1a,b). Isotype IgG-MPIO negative control constructs did not bind to TNF- α -stimulated sEND-1 cells. To demonstrate specific retention further, we pre-incubated VCAM-MPIO with a chimeric protein containing the extracellular domain of VCAM-1 (Fc-VCAM-1). Blocking with this soluble ligand almost completely abolished subsequent VCAM-MPIO retention by TNF- α -stimulated sEND-1 cells. By contrast, pre-incubation with the soluble extracellular domain of intercellular cell adhesion molecule-1 (Fc-ICAM-1) had no effect on VCAM-MPIO retention, as assessed by confocal microscopy (Fig. 1c,d).

Flow cytometry confirmed that sEND-1 cells had low basal expression of VCAM-1, but showed strong upregulation of VCAM-1 with TNF- α (Fig. 2a). Pre-incubation of VCAM-1 antibody with soluble Fc-VCAM-1 specifically inhibited VCAM-1 binding, whereas pre-incubation of VCAM-1 antibody with Fc-ICAM-1 had no effect (Fig. 2b,c).

In vivo MRI detects VCAM-MPIO bound to brain endothelium

To induce endothelial activation and VCAM-1 expression *in vivo*, mice were given interleukin-1 β (IL-1 β) by unilateral stereotaxic

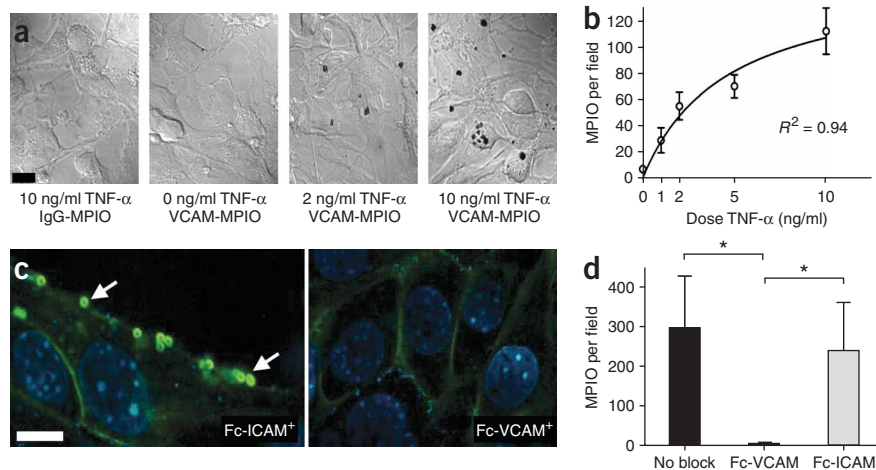


Figure 1 MPIO binding to cultured sEND-1 cells. (a) After stimulation with TNF- α (0–10 ng/ml), cells were exposed to VCAM-MPIO or isotype IgG-MPIO. In the absence of TNF- α , there was minimal VCAM-MPIO retention by sEND-1 cells. Scale bar, 10 μ m. (b) Dose-dependent retention of VCAM-MPIO in response to incremental doses of TNF- α ($R^2 = 0.94$, $P < 0.01$). Binding persisted after extensive washing and was restricted to cellular areas. (c) Confocal microscopy of sEND-1 cells stimulated with TNF- α (50 ng/ml). Green fluorescence reflects expression of VCAM-1 on the cell surface. Prior incubation of VCAM-MPIO with Fc-ICAM-1 had no effect on VCAM-MPIO binding (autofluorescent yellow-green spheres, arrows), whereas pre-incubation with Fc-VCAM-1 abolished VCAM-MPIO retention by cells almost completely, despite demonstrable surface expression of VCAM-1. sEND-1 cell nuclei are stained blue. Scale bar, 5 μ m. (d) Retained VCAM-MPIO (mean \pm s.d.) after TNF- α stimulation with and without pre-incubation with soluble Fc-VCAM-1 or Fc-ICAM-1 (* $P < 0.0001$).

micro-injection to the left striatum. We subsequently administered antibody-MPIO constructs systemically by tail vein injection. Circulation time allowed for both specific binding in the brain and clearance of unbound contrast from the blood. Mice underwent MRI, under general anesthesia, 4.5–5.5 h after injection of IL-1 β and 1.5–2.0 h after administration of contrast agent.

VCAM-MPIO caused a marked MRI contrast effect manifest as intensely low signal areas that appeared to delineate blood vessels on the IL-1 β -injected side of the brain. Nonspecific retention was almost absent from the non-injected hemisphere (Figs. 3 and 4 and Supplementary Video 1 online). The dynamics of leukocyte-endothelial binding are complex and depend on multiple ligand-receptor interactions. To mimic leukocyte binding more closely, dual antibody-conjugated MPIO were constructed, targeting both VCAM-1 and P-selectin. These dual antibody-conjugated MPIO also bound specifically but did not further enhance contrast effects (Fig. 3b). Control mice that underwent the same injection regime with an irrelevant isotype antibody-conjugated MPIO showed no contrast effect (Fig. 3c).

Pre-treatment of mice with VCAM-1 antibody 30 min before VCAM-MPIO administration abolished retention of VCAM-MPIO despite IL-1 β injection (Figs. 3d and 4b and Supplementary Video 2 online). Similarly, control mice (with no intracerebral injection

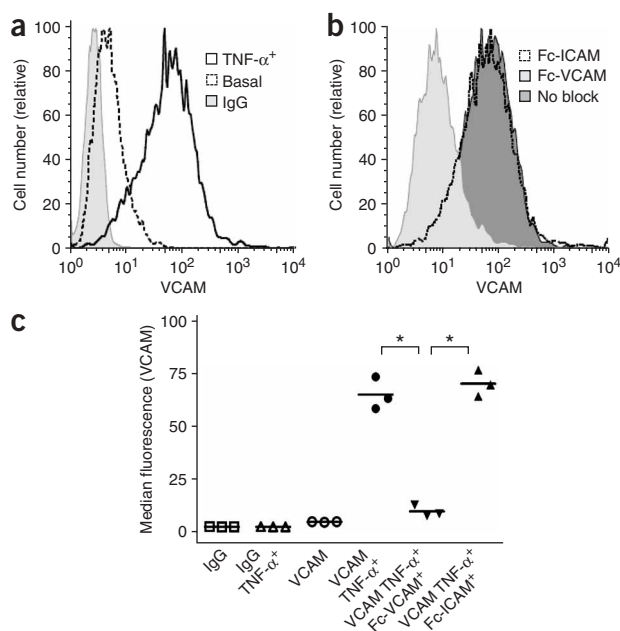


Figure 2 Flow cytometry. (a) Low basal expression of VCAM-1 by sEND-1 cells with marked upregulation in response to TNF- α . (b) Fc-VCAM-1 potently and specifically inhibited the interaction of VCAM-1 antibody with sEND-1 cells, whereas Fc-ICAM-1 had no effect. (c) Quantitative analysis confirmed the absence of nonspecific binding of IgG-MPIO both basally (IgG) and in the presence of TNF- α (IgG TNF- α ⁺), and low VCAM-1 expression under basal conditions (VCAM) with marked upregulation after TNF- α stimulation (VCAM TNF- α ⁺). Antibody binding to VCAM was almost completely abrogated by Fc-VCAM-1, whereas Fc-ICAM-1 had no effect (* $P < 0.001$).

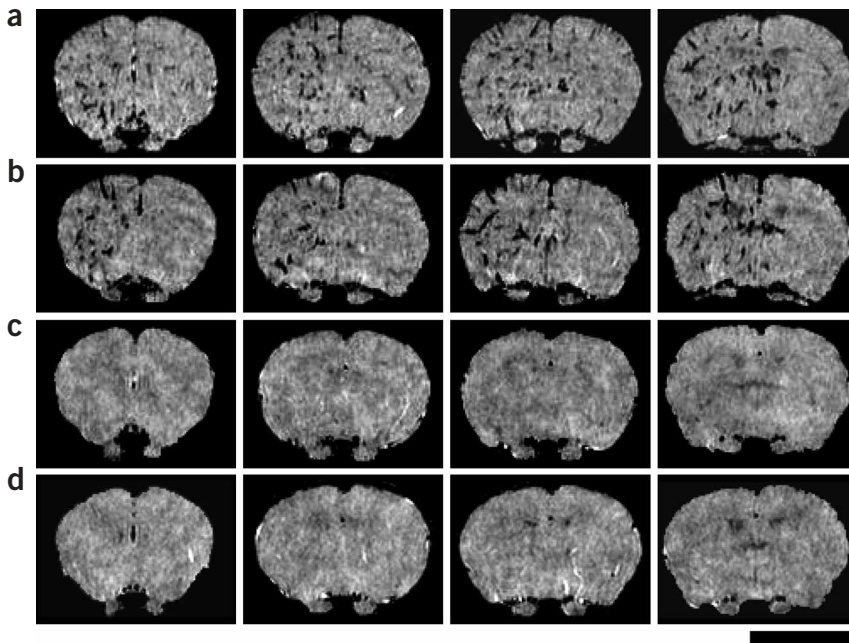


Figure 3 *In vivo* T₂*-weighted coronal images from 3D gradient echo data sets each with ~90-μm isotropic resolution. Four images are shown per brain. (a) Mouse injected intrastrially with 1 ng of IL-1β in 1 μl of saline 3 h before intravenous injection of VCAM-MPIO (~4.5 mg iron per kg). Intense low signal areas (black) on the left side of the brain reflect the specific MPIO retention on acutely activated vascular endothelium with almost absent contrast effect in the contralateral control hemisphere. (b) Similar, unilateral MPIO contrast effects in a mouse injected as in a but with VCAM+P-selectin-MPIO. (c) Absence of MPIO effects in a mouse injected as in a but with IgG-MPIO control. (d) Absence of MPIO effects in a mouse injected with IL-1β into the striatum and with VCAM-MPIO intravenously after pretreatment with VCAM-1 antibody, which effectively blocked VCAM-MPIO binding. In a–d, MRI data were obtained 1–2 h after MPIO injection. Scale bar, 5 mm.

or with injection of normal saline vehicle only) that received VCAM-MPIO systemically showed no specific contrast effects.

To appreciate the extent and architecture of the contrast effect, segmented areas were rendered to create a three-dimensional (3D) volumetric map of contrast binding that clearly demonstrated delineation of vascular structures in the IL-1β-stimulated hemisphere and almost total absence of binding on the contralateral, non-activated side (Fig. 4a). Pre-treatment to block VCAM-1 abolished VCAM-MPIO retention (Fig. 4b).

Quantitative analysis of MPIO binding

As compared with brains without IL-1β injection, specific contrast was increased more than 100-fold ($3,999 \pm 1,959 \times 10^{-6} \mu\text{m}^3$ versus $36 \pm 94 \times 10^{-6} \mu\text{m}^3$, mean \pm s.d.; $P = 0.02$) after administration of VCAM-MPIO. No further increase in specific contrast was observed for the dual VCAM and P-selectin antibody-conjugated MPIO (Fig. 4c).

Distribution of MPIO on histology

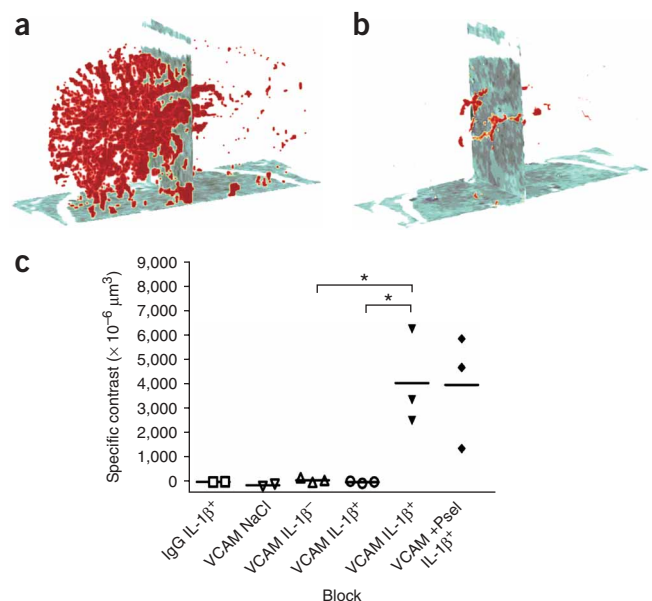
Histological examination indicated that VCAM-MPIO lined venules in the IL-1β-stimulated hemisphere (47 ± 15 per section) and

showed sparse retention in the contralateral, non-activated hemisphere (3 ± 4 , $P < 0.0001$; Fig. 5). MPIO were confined to the lumen of the vessel without extravasation. Isolated MPIO were the most common finding. Small clusters, similar to those seen *in vitro*, were present in relatively small numbers (Fig. 5b,c). Phagocytic cells with MPIO within their cytoplasm were occasionally identified. Expression of VCAM-1 was confirmed by immunohistochemistry, showing a distribution that was limited to vascular endothelium (Fig. 5b).

Safety and tolerability

Injection of antibody-conjugated MPIO was well tolerated in all mice. None of the 16 mice showed signs of ill effect during close observation for up to 5 h after injection.

Figure 4 Three-dimensional volumetric maps of VCAM-MPIO binding and quantitative analyses of MPIO contrast effects. VCAM-MPIO is shown in red. (a) In each mouse, 41 contiguous images were segmented by an automated analysis of signal intensity histograms. MPIO contrast effects delineated the architecture of cerebral vasculature in the IL-1β-stimulated hemisphere (left half of image) with almost total absence of binding on the contralateral, non-activated side. The midlines are indicated by vertical sections. (b) Pre-administration of VCAM-1 antibody abolished VCAM-MPIO retention. (c) As compared with brains without IL-1β injection, specific contrast was increased >100-fold after administration of VCAM-MPIO. Dual conjugated MPIO targeting both VCAM-1 and P-selectin also bound specifically but did not further enhance contrast effects. Substitution of IgG-MPIO (IgG/IL-1β⁺), sham intracerebral injection (VCAM/NaCl), no intracerebral injection (VCAM/IL-1β⁻) and pre-blocking (VCAM/IL-1β⁺ with block) were not associated with specific contrast effects. Bars indicate mean values for each group (* $P = 0.02$).



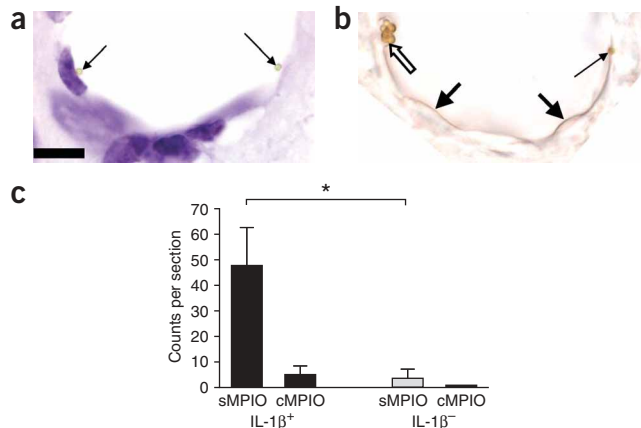


Figure 5 Postmortem light micrographs of mouse brain. (a) Cresyl violet staining shows MPIO lining a venule on the injected side of the brain. MPIO were confined to the lumen of the vessel (thin arrows). Binding most often comprised isolated MPIO. (b) Occasional clusters of MPIO were seen (clear arrow), some of which appeared to reflect phagocytic cells with MPIO within their cytoplasm. Presence of VCAM-1 (brown) was confirmed by immunohistochemistry, which showed expression limited to vascular endothelium (large arrows) and colocalization of VCAM-1 immunostaining and *in vivo* VCAM-MPIO binding. (c) Quantification of MPIO binding in the IL-1 β -stimulated (IL-1 β ⁺) and unstimulated hemispheres of mice receiving VCAM-MPIO demonstrated retention of MPIO in the former with a strong preponderance of single MPIO particles (sMPIO) with less frequent clusters (cMPIO; * $P < 0.0001$). Scale bar, 10 μ m.

DISCUSSION

We have reported the development and application of a molecular imaging probe that facilitates the identification of VCAM-1 expression in mouse brain *in vivo* by MRI. The specificity and potency of the contrast effects are marked and derive from a combination of targeted delivery of a large amount of iron oxide to sites of early inflammation and rapid clearance of MPIO from the blood.

The appeals of this approach are manifold. In the context of multiple sclerosis, this technique images a process that occurs early in disease pathogenesis. Unlike existing techniques, our approach does not require tissue destruction or compromise to the blood-brain barrier. Inhibiting the interaction between leukocytes and VCAM-1 has clinical benefit¹¹, and the ability to image VCAM-1 raises the possibility of targeting treatment to individuals with increased VCAM-1 expression.

VCAM-1 participates in other inflammatory conditions, including atherogenesis^{14,15}, transplant rejection¹⁶ and cancer¹⁷, for which therapeutic VCAM-1 targeting may also be effective^{18,19}. More broadly, by modifying the ligand, MPIO constructs could readily be adapted to image other endothelial targets that are differentially expressed in a broad range of pathologies.

Ultrasound has shown promise for imaging endothelial molecules with targeted microbubbles²⁰, and an enhanced technique using sensitive particle acoustic quantification has been applied to measure ICAM-1 and VCAM-1 in rat brain²¹. Ultrasound techniques are, however, inherently limited by the need for acoustic windows and ultrasound cannot reliably penetrate human skull. By contrast, MRI provides exquisite spatial resolution and tissue contrast, without ionizing radiation, making it the imaging modality of choice for many brain pathologies and driving the need for molecular magnetic resonance contrast.

Gadolinium-based contrast agents shorten T_1 , providing positive contrast on T_1 -weighted images²². Expression of ICAM-1 in rat brain has been imaged *ex vivo* by using paramagnetic liposomes²³, and we have targeted E-selectin expression in rat brain *in vivo* by using a sialyl Lewis^x moiety conjugated to Gd-DTPA²⁴. The small quantity of gadolinium that can be delivered to an endothelial monolayer, however, limits its contrast effect. By comparison, USPIO provide greater contrast but may require sophisticated ligands that mediate internalization by endothelial cells to achieve adequate local concentrations²⁵. USPIO have become popular owing to their long half-life in blood, which is a positive attribute for applications such as the measurement of changes in cerebral perfusion. This property is more of a hindrance in targeted contrast agents, however, because it leads to high background contrast for an extended period. A further potential drawback of USPIO is that contrast is manifest in T_2^* -weighted images as indistinct areas of low signal that can be difficult to distinguish from the ordinary heterogeneity of normal tissue. In addition, because USPIO can be taken up nonspecifically by endothelial cells, there is potential to compromise the specificity of molecular targeting¹³.

MPIO convey an amount of iron that is orders of magnitude greater than USPIO, and cause a local magnetic field inhomogeneity extending for a distance roughly 50 times their physical diameter¹². Although smaller than leukocytes and thus not prone to small-vessel plugging, MPIO preclude translocation across the endothelium owing to their size and incompressible nature, as confirmed by histology. The pattern of MPIO binding appeared almost identical to the patterns of lymphocyte binding in venules in the rat experimental autoimmune encephalomyelitis model of multiple sclerosis¹⁰.

Trials have demonstrated clear clinical benefits from inhibition of the interaction between VCAM-1 and its ligand¹¹. The ability to image VCAM-1 expression, in conjunction with existing diagnostic approaches, may offer clinically important opportunities to enhance specificity and to accelerate diagnosis. Early diagnosis and delivery of specific guided intervention may improve outcomes and allow response to treatment to be more precisely monitored.

Our approach uses commercially available reagents to provide a generic platform technology for endovascular molecular MRI and potentially allows the substitution of alternative ligands. With respect to translation to clinical use, our approach has three key factors. First, MPIO size. At the doses used here, short-term ill effects were not seen in mice, nor was there evidence of tissue infarction owing to small-vessel plugging. Indeed *in vivo* imaging and subsequent histological analysis of non-injected hemispheres both confirmed that nonspecific MPIO retention was minor. Second, MPIO composition. The MPIO used here are nonbiodegradable and are not suitable for use in humans. Iron oxide-containing contrast media are, however, in clinical use, and it should be feasible to synthesize biodegradable particles^{26,27}. Third, iron dose. The dose of iron (4.5 mg iron per kg (body weight)) reflects closely the dose of 2.6 mg per kg that has been used extensively for human oncological MRI with USPIO²⁸, and is considerably less than that used (30 mg per kg) in a study targeting USPIO to image VCAM-1 in mice²⁵.

In conclusion, this molecular imaging approach manifests exceptionally potent contrast effects in MRI. In a mouse model of acute inflammation, cerebral blood vessels were delineated and VCAM-MPIO binding was quantified. Alternative ligand-MPIO constructs provide clear opportunities for diagnostic imaging using specific endothelial cell markers that are differentially expressed in various pathologies, including inflammatory diseases, cancer and atherothrombosis.

METHODS

Antibody conjugation to MPIO. We used myOne tosylactivated MPIO (1- μ m diameter; iron content 26%) with *p*-toluenesulphonyl (tosyl)-reactive surface groups (Invitrogen) for antibody conjugation. We washed MPIO with sodium borate buffer (0.1 M, pH 9.5) and added purified monoclonal rat antibodies specific to mouse VCAM-1 (clone M/K2, Cambridge Bioscience), IgG-1 (clone Lo-DNP-1, Serotec) or a combination (50/50 wt/wt) of VCAM-1 and P-selectin (clone RB40.34, Fitzgerald Industries; 1×10^9 MPIO per 40 μ g of antibody for all). We added 3 M ammonium sulfate to give a final concentration of 1 M. We incubated the solution with constant rotation at 37 °C for 20 h. After incubation, we collected MPIO by using a Dynal magnet (Invitrogen) and discarded the supernatant containing any unbound antibody. We added PBS plus 0.5% BSA and 0.05% Tween 20 (pH 7.4) and incubated MPIO at 37 °C overnight to block the remaining active tosyl sites. We washed MPIO with PBS plus 0.1% BSA and 0.05% Tween 20 at 4 °C before storing at a concentration of 2.5×10^{10} MPIO per ml of PBS plus 0.1% BSA and 0.05% Tween 20 at 4 °C. We calculated that the primary amine and sulfhydryl groups of 1- μ m tosylactivated MPIO have a capacity to bind covalently 1.8×10^9 IgG molecules per MPIO.

Mouse protocol. After anesthesia with isofluorane (2.0–2.5% in 70% N₂O:30% O₂), adult male NMRI mice (35 \pm 2 g) were placed in a stereotaxic frame under a Wild M650 operating microscope (Leica). Using a glass pipette (tip <50 μ m), we stereotaxically injected 1 ng of mouse recombinant IL-1 β in 1 μ l of low endotoxin saline into the left striatum (coordinates from Bregma: anterior 0.5 mm, lateral 2 mm, depth 2.5 mm), to induce endothelial activation. After 3.1 \pm 0.2 h, we injected mice through a tail vein with VCAM-MPIO, VCAM+P-selectin-MPIO, or IgG-MPIO (4×10^8 microparticles; \sim 4.5 mg iron per kg; $n = 3$ per group). We had two control groups of mice ($n = 2$ per group): in one, mice were injected intracerebrally with 1 μ l of low endotoxin saline; in the other, mice were not injected intracerebrally. We subsequently administered VCAM-MPIO intravenously to both control groups. To determine selectivity of VCAM-MPIO, we injected a further group of mice ($n = 3$) with 0.2 mg of VCAM-1 antibody per kg at 3.3 \pm 0.4 h after intracerebral IL-1 β injection to block VCAM-1-binding sites. We subsequently administered VCAM-MPIO 15 min later. After VCAM-MPIO injection, mice were placed in a quadrature birdcage coil with an in-built stereotaxic frame for imaging. We maintained anesthesia with 1.5–1.8% isofluorane in 70% N₂O/30% O₂, monitored electrocardiography, and maintained body temperature at \sim 37 °C with a circulating warm water system. All procedures were approved by the UK Home Office.

In vivo MRI. We used a 7-Tesla horizontal bore magnet with an Inova spectrometer (Varian) to acquire a T_2^* -weighted 3D gradient echo data set with the following parameters: flip angle, 35°; repetition time, 50 ms; echo time, 5 ms; field of view, 22.5 \times 22.5 \times 31.6 mm³; matrix size, 192 \times 192 \times 360; two averages; total acquisition time, \sim 1 h. The mid-point of acquisition was 1.7 \pm 0.5 h after MPIO injection. We serially imaged the same mouse and found maximal contrast at 1–2 h with diminution by 4 h (data not shown). We zero-filled the data to 256 \times 256 \times 360 and reconstructed it off-line, giving a final isotropic resolution of 88 μ m³.

MRI analysis. For each magnetic resonance image, we manually masked the brain to exclude extracerebral structures. We segmented low-signal areas in 41 contiguous images, spanning a depth of 3.6 mm from the dorsal hippocampus ventrally. To control for minor variations in absolute signal intensity between individual scans, we calibrated low-signal areas on ten evenly spaced slices per brain. We applied the median signal intensity value to the fully automated, histogram-based batch analysis of the 41-slice sequence. We extracted data for left and right sides of the brain simultaneously with identical parameters. We summated voxel volumes and expressed them as raw volumes in cubic micrometers without surface rendering or smoothing effects. To ensure true laterality, we quantified contrast in each hemisphere 1 mm from the midline outwards. ImagePro Plus (Media Cybernetics) was used to segment and to quantify contrast volume by an operator who was blind to the origin of all data. We present the data as 'specific contrast', defined as 'left' minus 'right' contrast volume.

Additional methods. Information on cell culture and histology is available in the **Supplementary Methods** online.

Statistical analysis. Data are expressed as mean \pm s.d. and compared, where indicated, by two-tailed *t*-tests. We assigned statistical significance at $P < 0.05$.

Note: Supplementary information is available on the Nature Medicine website.

ACKNOWLEDGMENTS

We thank W. N. Haining for expertise in FACS analysis; T. Bannister for image analysis; D.R. Greaves for critical appraisal of the manuscript; and P. Townsend for overall laboratory management. This work was funded by the Wellcome Trust (R.P.C.) and the Medical Research Council (N.R.S. and D.C.A.).

AUTHOR CONTRIBUTIONS

R.P.C. and M.A.M. designed the contrast agent. M.A.M. manufactured the contrast agent and, in conjunction with N.W., K.M.C., C.v.z.M. and J.E.S., undertook the *in vitro* experiments. N.R.S., D.C.A., R.P.C. and M.A.M. designed the *in vivo* experiments. N.R.S., A.S.L. and D.C.A. conducted the MRI component, and C.v.z.M. and D.C.A. undertook histological analysis. R.P.C. supervised image analysis and analyzed the data. M.A.M., N.R.S. and R.P.C. contributed to the writing of the manuscript, and all authors discussed and refined the manuscript.

COMPETING INTERESTS STATEMENT

The authors declare competing financial interests: details accompany the full-text HTML version of the paper at www.nature.com/naturemedicine/.

Published online at <http://www.nature.com/naturemedicine>

Reprints and permissions information is available online at <http://npg.nature.com/reprintsandpermissions>

- Compston, A. & Coles, A. Multiple sclerosis. *Lancet* **359**, 1221–1231 (2002).
- McDonald, W.I. *et al.* Recommended diagnostic criteria for multiple sclerosis: guidelines from the International Panel on the Diagnosis of Multiple Sclerosis. *Ann. Neurol.* **50**, 121–127 (2001).
- Polman, C.H. *et al.* Diagnostic criteria for multiple sclerosis: 2005 revisions to the 'McDonald Criteria'. *Ann. Neurol.* **58**, 840–846 (2005).
- Goldberg-Zimring, D., Mewes, A.U.J., Maddah, M. & Warfield, S.K. Diffusion tensor magnetic resonance imaging in multiple sclerosis. *J. Neuroimaging* **15**, 68S–81S (2005).
- Ropele, S. *et al.* A comparison of magnetization transfer ratio, magnetization transfer rate, and the native relaxation time of water protons related to relapsing-remitting multiple sclerosis. *AJNR Am. J. Neuroradiol.* **21**, 1885–1891 (2000).
- Bitsch, A. *et al.* Inflammatory CNS demyelination: histopathologic correlation with in vivo quantitative proton MR spectroscopy. *AJNR Am. J. Neuroradiol.* **20**, 1619–1627 (1999).
- Guttmann, C.R., Meier, D.S. & Holland, C.M. Can MRI reveal phenotypes of multiple sclerosis? *Magn. Reson. Imaging* **24**, 475–481 (2006).
- Elices, M.J. *et al.* VCAM-1 on activated endothelium interacts with the leukocyte integrin VLA-4 at a site distinct from the VLA-4/fibronectin binding site. *Cell* **60**, 577–584 (1990).
- Carlos, T.M. *et al.* Vascular cell adhesion molecule-1 mediates lymphocyte adherence to cytokine-activated cultured human endothelial cells. *Blood* **76**, 965–970 (1990).
- Yednock, T.A. *et al.* Prevention of experimental autoimmune encephalomyelitis by antibodies against $\alpha_4\beta_1$ integrin. *Nature* **356**, 63–66 (1992).
- Polman, C.H. *et al.* A randomized, placebo-controlled trial of natalizumab for relapsing multiple sclerosis. *N. Engl. J. Med.* **354**, 899–910 (2006).
- Shapiro, E.M. *et al.* MRI detection of single particles for cellular imaging. *Proc. Natl. Acad. Sci. USA* **101**, 10901–10906 (2004).
- Briley-Saebo, K. *et al.* Hepatic cellular distribution and degradation of iron oxide nanoparticles following single intravenous injection in rats: implications for magnetic resonance imaging. *Cell Tissue Res.* **316**, 315–323 (2004).
- Cybulsky, M.I. *et al.* A major role for VCAM-1, but not ICAM-1, in early atherosclerosis. *J. Clin. Invest.* **107**, 1255–1262 (2001).
- Nakashima, Y., Raines, E.W., Plump, A.S., Breslow, J.L. & Ross, R. Upregulation of VCAM-1 and ICAM-1 at atherosclerosis-prone sites on the endothelium in the ApoE-deficient mouse. *Arterioscler. Thromb. Vasc. Biol.* **18**, 842–851 (1998).
- Orosz, C.G. *et al.* Role of the endothelial adhesion molecule VCAM in murine cardiac allograft rejection. *Immunol. Lett.* **32**, 7–12 (1992).
- Maurer, C.A. *et al.* Over-expression of ICAM-1, VCAM-1 and ELAM-1 might influence tumor progression in colorectal cancer. *Int. J. Cancer* **79**, 76–81 (1998).
- Dedrick, R.L., Bodary, S. & Garovoy, M.R. Adhesion molecules as therapeutic targets for autoimmune diseases and transplant rejection. *Expert Opin. Biol. Ther.* **3**, 85–95 (2003).
- Gosk, S., Gottstein, C. & Bendas, G. Targeting of immunoliposomes to endothelial cells expressing VCAM: a future strategy in cancer therapy. *Int. J. Clin. Pharmacol. Ther.* **43**, 581–582 (2005).

20. Villanueva, F.S. *et al.* Microbubbles targeted to intercellular adhesion molecule-1 bind to activated coronary artery endothelial cells. *Circulation* **98**, 1–5 (1998).
21. Reinhardt, M. *et al.* Ultrasound derived imaging and quantification of cell adhesion molecules in experimental autoimmune encephalomyelitis (EAE) by Sensitive Particle Acoustic Quantification (SPAQ). *Neuroimage* **27**, 267–278 (2005).
22. Aime, S. *et al.* Insights into the use of paramagnetic Gd(III) complexes in MR-molecular imaging investigations. *J. Magn. Reson. Imaging* **16**, 394–406 (2002).
23. Sipkins, D.A. *et al.* ICAM-1 expression in autoimmune encephalitis visualized using magnetic resonance imaging. *J. Neuroimmunol.* **104**, 1–9 (2000).
24. Sibson, N.R. *et al.* MRI detection of early endothelial activation in brain inflammation. *Magn. Reson. Med.* **51**, 248–252 (2004).
25. Nahrendorf, M. *et al.* Noninvasive vascular cell adhesion molecule-1 imaging identifies inflammatory activation of cells in atherosclerosis. *Circulation* **114**, 1504–1511 (2006).
26. Sakhalkar, H.S. *et al.* Leukocyte-inspired biodegradable particles that selectively and avidly adhere to inflamed endothelium in vitro and in vivo. *Proc. Natl. Acad. Sci. USA* **100**, 15895–15900 (2003).
27. Chen, H.H. *et al.* MR imaging of biodegradable polymeric microparticles: a potential method of monitoring local drug delivery. *Magn. Reson. Med.* **53**, 614–620 (2005).
28. Will, O. *et al.* Diagnostic precision of nanoparticle-enhanced MRI for lymph-node metastases: a meta-analysis. *Lancet Oncol.* **7**, 52–60 (2006).